This article has been accepted for publication in IEEE Journal of Biomedical and Health Informatics. This is the author's version which has not been fully edited and content may change prior to final publication. Citation information: DOI 10.1109/JBHI.2024.3463737

Lightweight Source-Free Domain Adaptation based on Adaptive Euclidean Alignment for Brain-Computer Interfaces

Huiyang Wang, Hongfang Han, John Q. Gan, and Haixian Wang, *Senior Member, IEEE*

***Abstract*—For privacy protection of subjects in electroencephalogram (EEG)-based brain-computer interfaces (BCIs), using source-free domain adaptation (SFDA) for cross-subject recognition has proven to be highly effective. However, updating and storing a model trained on source subjects for each new subject can be inconvenient. This paper extends Euclidean alignment (EA) to propose adaptive Euclidean alignment (AEA), which learns a projection matrix to align the distribution of the target subject with the source subjects, thus eliminating domain drift issues and improving model classification performance of subject-independent BCIs. Combining the proposed AEA with various existing SFDA methods, such as SHOT, GSFDA, and NRC, this paper presents three new methods: AEA-SHOT, AEA-GSFDA, and AEA-NRC. In our experimental studies, these AEA-based SFDA methods were applied to four well-known deep learning models (*i.e.*, EEGNet, Shallow ConvNet, Deep ConvNet, and MSFBCNN) on two motor imagery (MI) datasets, one event-related potential (ERP) dataset and one steady-state visual evoked potentials (SSVEP) dataset. The advanced cross-subject EEG classification performance demonstrates the efficacy of our proposed methods. For example, AEA-SHOT achieved the best average accuracy of 81.4% on the PhysioNet dataset.**

***Index Terms* — Electroencephalogram (EEG), brain-computer interfaces, domain adaptation, source-free domain adaptation, deep learning**

I. Introduction

This work was supported by the National Natural Science Foundation of China under Grants 92270113 and 62176054 (*Corresponding author: Haixian Wang*).

Huiyang Wang and Haixian Wang are with the Key Laboratory of Child Development and Learning Science of Ministry of Education, School of Biological Science & Medical Engineering, Southeast University, Nanjing 210096, Jiangsu, PR China (e-mail: stickovercarrot@foxmail.com; hxwang@seu.edu.cn).

Hongfang Han is with the School of Computer Science and Information Engineering, Shanghai Institute of Technology, Shanghai 201418, China (e-mail: hanhf@sit.edu.cn)

John Q. Gan is with the School of Computer Science and Electronic Engineering, University of Essex, Colchester CO4 3SQ, UK (e-mail: jqgan@essex.ac.uk).

Electroencephalogram (EEG) signals are pivotal in brain-computer interfaces (BCIs) that translate brain activities into meaningful information to facilitate communication between the brain and external environments [1][2]. EEG-based BCIs are based on motor imagery (MI) classification [3][4], event-related potential (ERP) recognition [5][6], or steady-state visual evoked potentials (SSVEP) analysis [7][8] and have found many applications including healthcare such as seizure detection [9][10]. However, the low signal-to-noise ratio (SNR) of EEG signals and the intricacies of cognitive processes within the brain make the decoding of mental activities in EEG-based BCIs a very challenging problem [11].

Due to the significant advancements in deep learning, the EEG decoding performance based on various neural network models has dramatically improved. Some studies have achieved average accuracies exceeding 95% in four-class MI tasks [12][13]. However, the substantial variance across different subjects makes it impossible to create a universally optimal model suitable for all individuals. It requires collecting data from target (new) subjects to fine-tune a pre-trained model (in this paper, a model trained before the target subjects is referred to as a pre-trained model for convenience). Utilizing unlabelled data from the target subjects to enhance the performance of pre-trained models in the target domain has garnered significant attention from researchers [14][15], which is a suitable and natural choice for various EEG-based BCIs. For instance, as a new user engages with the system through motor imagery, their unlabelled data accumulates over time. Transfer learning, or domain adaptation (DA), is widely used to improve model performance by making use of unlabelled data. The mainstream idea of DA is aligning the data from the target domain and source domain in a feature space, such as in CDAN [16], DANN [17], and deep CORAL [18]. Another widely used idea in the EEG field is covariance matrix alignment, which makes the covariance matrices of the source and target domains equal and independent of deep learning [19][20].

To protect source subjects' privacy, data from source subjects is sometimes unavailable during domain adaptation. In such cases, source-free domain adaptation (SFDA) is useful for extending knowledge to target subjects by only relying on a model trained on source subjects (pre-trained model) [21][22]. A popular idea of SFDA is to use the expected output of the target domain. Specifically, the distribution of target domain features extracted by the pre-trained model is in line with predefined

rules, such as forming multiple clusters by category, with each cluster having a uniform sample distribution [23]. Consequently, updating the weights of pre-trained models is essential to achieve competitive results, whether with images, natural language, or EEG. Updating a pre-trained model for each new subject is not storage-efficient. Fortunately, at least in the EEG field, there are covariance matrix alignment methods that do not necessitate updating models.

Inspired by Euclidean alignment (EA) [24], this paper proposes adaptive Euclidean alignment (AEA) and applies it to traditional SFDA methods. AEA and SFDA mutually address each other's limitations. On the one hand, AEA addresses the drawback of relying on source data to compute the projection matrix through SFDA. On the other hand, SFDA ensures improved classification performance in the target domain without updating the weights of pre-trained models through AEA, thus significantly reducing storage space and time for retraining models. The main contributions of this paper are as follows:

1) This paper proposes AEA-based SFDA methods, which require learning only a projection matrix end-to-end to align the distribution of the target domain with the source domain. For AEA, source domain data is not required; For SFDA, there is no need to update the weights of the pre-trained model. These settings differ from existing EA and traditional SFDA methods. To our knowledge, this approach has not been studied before.
2) This paper combines the proposed AEA with three classic SFDA algorithms, which were validated using four benchmark models on four public datasets (two MI, one ERP, and one SSVEP). The experimental results have consistently demonstrated the effectiveness of the AEA.
3) This paper shows that the proposed AEA can increase the efficiency of multi-subject inference.
4) This paper is the first to investigate source-free transfer learning in scenarios where source and target domain data processing is not strictly consistent. This is beneficial for assessing the robustness and adaptability of our methods in various unknown adverse conditions.

II. Related Work

Source-free domain adaptation only uses unlabelled target data without access to source data to fine-tune models trained on the source domain. The first branch of SFDA methods is based on self-training. SHOT [23] uses a mutual information maximization strategy to generate balanced and clustered outputs in the target domain. GSFDA [25] and NRC [26] take into account the supervision of neighborhood samples, as they believe that the class of a sample, along with its neighbors, should remain consistent. BAIT [27] and A^{2}Net [28] both perform adversarial training. The former uses wandering samples, similar to support vectors in support vector machines (SVM), to train a classifier that makes opposite predictions to the source classifier and then encourages the feature extractor to make the two classifiers get consensus; The latter finds source-similar target samples and adopts soft-adversarial manner with the introduced target classifier to eliminate the discrepancy between source-similar and source-dissimilar samples. The other branch of SFDA methods is based on generative models, which share a relatively unified idea: they use pre-trained models to generate synthetic target-style training data, enabling the application of existing domain adaptation methods for transfer [29][30]. There are also many remarkable studies related to SFDA in the EEG field. Guney et al. [31] use neighborhood supervision similar to NRC's to address the source-free transfer problem in SSVEP. Xia et al. [32] consider the impact of class imbalance and sample importance in MI transfer to improve Tsallis entropy. It helps reduce the uncertainty of pre-trained models for predicting target data. Zhao et al. [33] use ensemble learning to enhance the effectiveness of SFDA in epilepsy detection. All the methods mentioned above rely on updating pre-trained models to work better. The work in this paper aims to overcome this limitation.

Covariance matrix alignment involves aligning raw EEG signals across domains without concerning models, thus allowing the pre-trained model's weights to be retained. The Riemannian alignment (RA) framework aligns the EEG covariance matrices from different subjects or sessions in the Riemannian space [34]. She et al. [14] extend the RA method, which minimizes the marginal probability distribution on the Riemannian manifold and subsequently transfers the manifold features with conditional probability distribution adaptation. Maswanganyi et al. [35] apply RA to a selection of multiple source subjects and extend it to multi-class cases. On the other hand, the Euclidean alignment (EA) framework aligns the EEG covariance matrices in the Euclidean domain [24]. He and Wu [36] extend EA to different label spaces and move the per-class covariance matrices of each source subject, relocating them to the corresponding class center of the target subject. It is worth noting that when the aligned covariance matrices become an identity matrix by default, the EA for target data does not necessitate source data. However, source data processing generally does not consider future transfer learning.

Manual feature transfer is also commonly used in brain-computer interfaces. Dai et al. [37] proposed a transfer kernel common spatial pattern (TKCSP) to learn a domain-invariant kernel across subjects. TKCSP first utilizes kernel common spatial pattern (KCSP) [38] to extract components that maximize the energy between two classes and then matches distributions across subjects to learn a domain-invariant kernel by transfer kernel learning (TKL) [39]. Lan et al. [40] utilized transfer component analysis (TCA) [41] to learn the transferable components across domains in a reproducing kernel Hilbert space (RKHS) for subject-independent emotion recognition. Zhang et al. [42] addressed the alignment of both marginal and conditional distributions between the source and target domains through joint distribution adaptation (JDA) [43]. They embedded manifold regularization into JDA to ensure the classifier can produce consistent outputs across both domains. Zhu et al. [44] designed a motor imagery transfer learning framework by combining weighted balanced distribution adaptation (W-BDA) [45], source empirical risk, and manifold regularization to reduce the variation in different subjects. Guan et al. [46] introduced general tensor discriminative analysis (GTDA) [47] to construct the objective function of class-wise discrimination learning to further enhance the effectiveness of cross-task mental workload recognition.

This article has been accepted for publication in IEEE Journal of Biomedical and Health Informatics. This is the author's version which has not been fully edited and content may change prior to final publication. Citation information: DOI 10.1109/JBHI.2024.3463737

III. METHODS

A. Definitions and Notations

A labeled source domain EEG dataset is defined as $D_s = \{(x_i, y_i)\}_i^{n_s}$, where $x_i \in R^{C\times M}$ represents the *i-th* trial with M discretized time points and C channels, n_s is the total number of source domain trials and $y_i \in \{1, 2, \cdots, K\}$ is the corresponding label of x_i, where K is the total number of classes. An unlabelled target domain EEG dataset is defined. $D_t = \{x_j\}_j^{n_t}$, where n_t is the total number of target domain trials. In a traditional DA setting, we make full use of both D_s and D_t to generalize a model from a source domain to a target domain. However, in the SFDA setting, the source domain samples D_s can only be available for model pre-training but not visible during the transfer task. This paper investigates deep learning models based on convolutional neural networks (CNNs), in which the last few layers form a classifier g, and the other layers are defined as a feature extractor f.

B. Euclidean Alignment (EA)

EA [24] assumes that the source and target domains should have consistent average covariance matrices, representing the distribution between each channel's time series. Therefore, EA finds projections to reduce the distance between the average covariance matrices of the source and target domains in the Euclidean space.

For the source domain D_s, EA calculates the covariance matrix for each EEG trail as follows:

$$Z_i = x_i x_i^T \tag{1}$$

and the average covariance matrix as

$$\bar{Z}_s = \frac{1}{n_s}\sum_{i=1}^{n_s} Z_i \tag{2}$$

The projection matrix is defined as

$$Q_s = \bar{Z}_s^{-1/2} \tag{3}$$

Similarly, EA calculates the projection matrix Q_t for the target domain D_t. Transferring the data distribution of the target domain to the source domain is performed as follows:

$$\tilde{x}_j = Q_s^{-1} Q_t x_j, \quad x_j \in D_t \tag{4}$$

Consequently, the average covariance matrix of $\{\tilde{x}_j\}_j^{n_t}$ is equal to $\bar{Z}_s$, achieving the goal of aligning domain data distributions of the target and source domains in the Euclidean space. However, due to unavailable D_s for privacy concerns, EA algorithms cannot be directly applied to the SFDA methods.

C. Adaptive Euclidean Alignment (AEA)

Eq. (4) can be rewritten as

$$\tilde{x}_j = P x_j \tag{5}$$

where $P = Q_t^{-1} Q_s$. While P cannot be directly computed, this paper leverages the learnability of deep learning models to propose adaptive Euclidean alignment for learning the projection matrix P. The core idea of AEA is to train P by the frozen pre-trained model and the loss function of the specific SFDA method. As shown in Fig. 1, the weights of the pre-trained model are not updated, but gradients are still backpropagated to update the projection matrix.

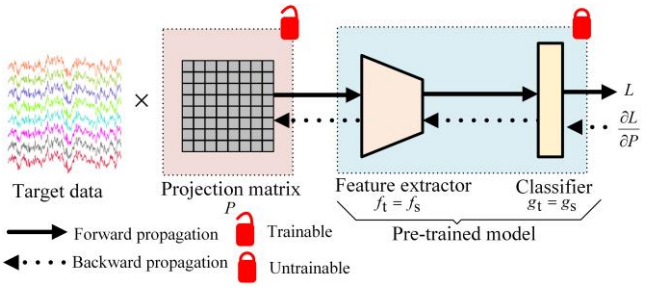

Fig. 1. The pipeline of AEA-based SFDA. During the transfer learning phase, only the projection matrix is updated. The loss function L depends on the specific SFDA method being used.

Frozen pre-trained model. Both the source classifier g_s and the source feature extractor f_s are frozen during SFDA, *i.e.*, $g_t = g_s$ and $f_t = f_s$. It is not only the essential difference between our proposed method and other existing SFDA methods but also a pivotal step to improve the domain adaptability of the pre-trained model. The classifier's weights should remain unchanged as it encodes the distribution information of unseen source data (hypothesis) [23]. It can be argued that the feature extractor only has the optimal feature mining ability in the source domain. However, after SFDA, its feature mining ability is weakened in the source domain and has limited improvement in the target domain without labeled data. This paper proposes to keep the advantages of the pre-trained model in the source domain and applies transfer learning to EEG data in the target domain by learning a projection matrix as P in eq. (5) such that the target data matches the source data distribution well, as shown in Fig. 2.

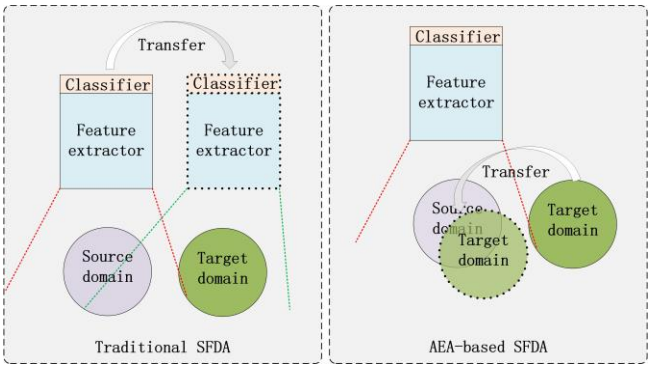

Fig. 2. The difference between traditional SFDA and AEA-based SFDA. (a) Traditional SFDA, in which the model weights are updated via transfer learning; (b) AEA-based SFDA, in which the target domain data distribution is changed, but there is no model updating. The range between red dashed lines represents the data distribution where the model performs best. In contrast, the range between green dashed lines represents the data distribution where the model achieves suboptimal performance after SFDA.

Loss function. The loss functions from the existing SFDA methods can be directly used to supervise the output distribution of the target domain, which will be used to

This article has been accepted for publication in IEEE Journal of Biomedical and Health Informatics. This is the author's version which has not been fully edited and content may change prior to final publication. Citation information: DOI 10.1109/JBHI.2024.3463737

learn the projection matrix P. The SFDA loss function typically consists of two components. The first component makes the target outputs globally diverse, ensuring an even distribution of the categories in the target domain, which is defined as follows:

$$L_{\text{div}} = \frac{1}{K}\sum_{k=1}^{K}\overline{p}_k \log \overline{p}_k \tag{6}$$

where $\overline{p}_k = \frac{1}{b}\sum_{i=1}^{b} p_{i,k}$, $p_{i,k} = \delta_k\left(g_t\left(f_t\left(Px_i\right)\right)\right)$, and δ_k represents the output of class k via the Softmax activation function, and b is the batch size. The second component aims to ensure confident predictions for each sample. The SHOT method adopts the following as the second component of its loss function:

$$L_{\text{ent}} = -\frac{1}{b}\sum_{i=1}^{b}\sum_{k=1}^{K} p_{i,k}\log p_{i,k} \tag{7}$$

The GSFDA method [25] incorporates local structure clustering (LSC) to group target features based on semantic proximity to ensure that samples and their immediate neighbors share the same labels. The second component of its loss function is defined as

$$L_{\text{lsc}} = -\frac{1}{b}\sum_{i=1}^{b}\sum_{j=1}^{m}\log\left(p_i \cdot \delta\left(\mathcal{N}_j\right)\right) \tag{8}$$

where $\mathcal{N}_j$ represents the feature vector with the $j\text{-}th$ smallest cosine distance from $f_t\left(Px_i\right)$, and m is the number of neighbors of $f_t\left(Px_i\right)$. The NRC method [26] is similar to GSFDA, but it takes into account the second-order neighborhood as well. The second component of its loss function is defined as

$$\begin{aligned} L_{\text{nrc}} = &-\frac{1}{b}\sum_{i=1}^{b}\sum_{j=1}^{m}\log\left(p_i \cdot \delta\left(\mathcal{N}_j\right)\right) \\ &-\frac{1}{b}\sum_{i=1}^{b}\sum_{j=1}^{m}\sum_{z=1}^{l} log\left(p_i \cdot \delta\left(\mathcal{M}_{j,z}\right)\right) \end{aligned} \tag{9}$$

where $\mathcal{M}_{j,z}$ represents the feature vector with the $z\text{-}th$ smallest cosine distance from $\mathcal{N}_j$, and l is the number of second-order neighbors.

The whole loss function of the three SFDA methods mentioned above can be expressed as

$$L = L_{\text{div}} + L_{\text{id}} \tag{10}$$

where L_{id} is L_{ent}, L_{lsc} or L_{nrc}. Therefore, updating P can be described by:

$$P \leftarrow P - \eta\frac{\partial L}{\partial P} \tag{11}$$

where η represents the learning rate.

Initialization of the projection matrix. According to eqs. (1)-(5), it is apparent that when the distributions of the target domain and the source domain are perfectly aligned, the projection matrix P becomes an identity matrix. Therefore, when the distribution disparity between the source and target domains is limited, fine-tuning P initialized by an identity matrix allows for a precise transformation of the target domain data. Another way is to initialize P with random values as follows:

$$P\left(i,j\right) = \begin{cases} 1 & if\ i == j \\ z \sim U\left(-a,a\right), & if\ i < j \\ P\left(j,i\right), & otherwise \end{cases} \tag{12}$$

The diagonal elements of P are still initialized to 1, while the initial values of the other elements follow a uniform distribution, *i.e.*, $P\left(i,j\right) \sim U\left(-a,a\right)$, and the value of a is set by default to 0.1 in this paper. It is worth noting that P is symmetric, so the learnable parameters include only the diagonal elements and the upper triangular elements. For a dataset with c channels, the number of learnable parameters in P is $\frac{c\left(c+1\right)}{2}$, which is usually significantly lower than the number of learnable parameters in a pre-trained model.

This paper proposes to combine AEA with SHOT (*i.e.*, $L_{\text{id}} = L_{\text{ent}}$), GSFDA (*i.e.*, $L_{\text{id}} = L_{\text{lsc}}$), and NRC (*i.e.*, $L_{\text{id}} = L_{\text{nrc}}$), respectively, leading to three AEA-based SFDA methods for domain adaptation in subject-independent BCIs, namely, AEA-SHOT, AEA-GSFDA, and AEA-NRC. One important detail to note is that SHOT freezes the weights of the classifier in the pre-trained model (*i.e.*, the weights of the last fully connected layer) and only updates the weights of the feature extractor (*i.e.*, the weights excluding the last fully connected layer). In contrast, GSFDA and NRC update all the weights of the pre-trained model. The pseudocode for updating the projection matrix in the proposed AEA-based methods is presented in Algorithm 1.

Algorithm 1

Initialize: Projection matrix P; Pre-trained model F.
Input: Unlabeled target domain EEG dataset $D_{\text{t}} = \left\{x_j\right\}_j^{n_{\text{t}}}$; Learning rate η; Training epochs N; Batch size b.
Output: Predict labels $\tilde{y}$ for target domain.

For i = 1, …, N **do**
  $\tilde{D}_{\text{t}} = D_{\text{t}}$
  For randomly selected $X = \left\{x_j\right\}_j^b$ from $\tilde{D}_{\text{t}}$ **do**
    Update $\tilde{D}_{\text{t}} \leftarrow \tilde{D}_{\text{t}} - X$
    $\tilde{X} = PX$
    $\tilde{y} = F\left(\tilde{X}\right)$
    Calculate the loss L according to eq. (10)
    Update $P \leftarrow P - \eta\frac{\partial L}{\partial P}$
    If $D_{\text{t}} == \varnothing$
      Break
    End if
  End do
End do

IV. Experiments

A. Datasets and Implementation Details

Two MI datasets, one ERP dataset and one SSVEP dataset were used in our experiments.

The first MI dataset is the High-Gamma Dataset (HGD) [48]. HGD consists of MI EEG data from 14 subjects. Each subject performed four MI tasks: left hand, right hand, both feet, and rest. For each subject, there are approximately 880 trials in the training set and approximately 160 trials in the testing set. 128-channel EEG signals were recorded at a 500 Hz sampling rate. In our experiments, following the approach described in [48], we selected only 44 EEG electrodes exhibiting a strong correlation with the motor imagery tasks for analysis. Each trial contains 0.5 seconds before the motion cue onset and lasts for 4.5 seconds. Additionally, we resampled the EEG signals to 250 Hz and applied a 0.5 Hz high-pass filter for signal filtering. An exponentially weighted moving average was employed for data preprocessing.

The second MI dataset is the PhysioNet dataset [49]. The PhysioNet dataset consists of MI EEG data from 109 subjects. Each subject performed five MI tasks, but we selected only four for experimentation: left fist, right fist, both feet, and rest. Eighty-four trials were recorded for each subject, and we randomly divided 70 trials as the training set, while the remaining trials were used as the testing set. 64-channel EEG signals were recorded at a 160 Hz sampling rate. Only 4 seconds in each trial (*i.e.*, from 1 to 5 seconds after the start of each trial) were utilized. Z-score standardization was used to preprocess the PhysioNet dataset.

The ERP dataset is a P300 Dataset (https://www.kaggle.com/datasets/rramele/p300samplingdataset). This dataset consists of ERP EEG data from 8 subjects, each participating in 35 trials. Each trial consists of seven five-letter words, with each letter being composed of 120 stimulations from the P300 matrix. These stimulations, organized in a six-row by six-column format, were repeated ten times to complete a trial. The goal is to decode four spelled words from the last 20 letters. 8 –channel EEG signals were recorded at a 250 Hz sampling rate. All signals were bandpass-filtered to a frequency range of 0.1 Hz to 24 Hz. The 1 s interval following the onset cue was selected for analysis. In our experiments, each subject had 620 target stimuli samples and 620 non-target stimuli samples. We allocated 1000 samples for training purposes, reserving the remaining samples for testing. Z-score standardization was used to preprocess the P300 dataset.

The SSVEP dataset is the Benchmark Dataset [51], which is composed of SSVEP EEG data from 35 subjects who participated in six blocks. Each block has 40 trials, with each trial representing a distinct target coded by a joint frequency and phase modulation (JFPM) approach. The stimulation frequency range is 8 to 15.8 Hz with an interval of 0.2 Hz, and the phase range is 0 to 1.5π with an interval of 0.5π. 64-channel EEG signals were recorded at a sampling rate of 250 Hz. This study uses data from 9 electrode channels: Pz, PO5, PO3, POz, PO4, PO6, O1, Oz, and O2 [31]. Each trial comprises 0.67 seconds following the onset of the target cue and spans a duration of 1 second. Following the previous studies [31], SSVEP data is filtered into three frequency bands: 8-15.8 Hz, 16-31.6 Hz, and 24-47.4 Hz. Therefore, SSVEP data requires learning three independent projection matrices, each used for the transformation of its corresponding frequency band.

Data setting. Leave-one-subject-out cross-validation was used for the HGD and P300 datasets to evaluate the classification performance. For the PhysioNet dataset, we only used the first 20 subjects. Among these, the first 10 subjects were used to train a pre-trained model, while the remaining 10 were individually employed for transfer learning. For the SSVEP dataset, the first 25 subjects were used to train a pre-trained model, while the remaining 10 were individually employed for transfer learning. In the pre-training phase, we trained the model by aggregating the training sets from multiple subjects. Using a target subject's training set, we trained P during the transfer learning phase. Subsequently, we preserved P that yielded the highest accuracy according to the target subject's testing set.

Model setting. For both MI and ERP tasks, we mainly employed the EEGNet [51] model as the backbone module, where the number of convolutional kernels in the first convolutional layer is 32 ($F1=32$). Additionally, we also evaluated AEA-based SFDA on DeepConv [48], ShallowConv [48], and MSFBCNN [52] models to further validate AEA's effectiveness and versatility in some experiments.

Hyper-parameters setting. The default initialization of P is based on the identity matrix. Stochastic gradient descent with the Adam update rule is used to train models. The learning rate was set to 0.001. The dropout probability and regularisation weight during the pre-training phase were set to 0.25 and 0.0005, respectively, whereas both were set to 0 during the transfer learning phase. The number of epochs was set to 200, and an early stopping strategy was adopted to avoid overtraining. The batch size is set to n_t to better optimize the loss L_{div} in eq. (6). Models were trained and tested in a PyTorch environment on an NVIDIA RTX 3090 graphics processing unit (GPU) for high-performance computing.

B. Classification Results on the MI Datasets

We used the EEGNet model for MI classification tasks to evaluate three AEA-based SFDA methods on two datasets. The MI classification results of AEA-based SFDA methods in comparison with those of the related state-of-the-art methods, with or without a source-free condition, are presented in Tables I and II. On the HGD dataset, AEA-SHOT and SHOT both achieved the highest average accuracy of 86.5%. Furthermore, AEA-SHOT demonstrated the most stable classification results among all subjects in terms of the standard deviation of accuracy. It is worth noting that the traditional EA achieved the poorest performance among all transfer learning methods. On the Physionet dataset, AEA-SHOT and AEA-NRC achieved the highest or the second-highest average accuracy, i.e., 81.4% and 80.7%, respectively. In addition, the average accuracy of DANN and CDAN is even lower than that of the non-transfer learning model, which could be attributed to the insufficient data of the Physionet dataset, leading to negative transfer.

This article has been accepted for publication in IEEE Journal of Biomedical and Health Informatics. This is the author's version which has not been fully edited and content may change prior to final publication. Citation information: DOI 10.1109/JBHI.2024.3463737

TABLE I
RESULTS ON HGD

Method	Source-free	1	2	3	4	5	6	7	8	9	10	11	12	13	14	Mean	Std
No TL	√	87.5	67.5	73.1	89.4	72.5	63.8	78.0	70.0	69.4	38.8	71.9	83.8	48.4	62.5	69.7	13.4
DANN* [16]	×	86.3	75.6	71.3	76.3	81.3	60.0	83.7	87.5	80.6	65.0	71.9	81.9	74.2	70.0	76.1	7.7
CDAN* [17]	×	88.8	68.8	79.4	79.4	82.5	63.1	82.4	88.8	80.6	65.0	71.3	81.3	71.7	66.3	76.4	8.3
EA* [24]	×	92.5	75.6	67.5	90.0	82.5	55.6	79.3	53.8	81.3	57.5	65.6	88.8	66.0	53.8	72.1	13.4
GSFDA* [25]	√	90.0	69.4	80.0	88.8	71.9	69.4	82.4	85.0	81.9	63.8	71.9	89.4	69.2	63.1	76.9	9.2
NRC* [26]	√	97.5	77.5	91.9	92.5	89.4	78.8	86.2	86.9	88.1	73.1	78.1	91.3	84.3	68.1	84.5	8.0
SHOT* [23]	√	96.3	79.4	95.0	96.9	96.3	78.1	91.2	90.6	89.4	83.1	73.8	90.6	76.7	73.8	**86.5**	8.4
AEA-GSFDA	√	93.1	76.9	89.4	93.8	83.1	68.1	83.0	89.4	83.8	78.8	73.1	88.8	76.7	67.5	81.8	8.3
AEA-NRC	√	90.0	84.4	79.4	95.0	89.4	70.6	83.0	86.9	85.0	83.1	74.4	93.1	74.8	81.3	83.6	6.9
AEA-SHOT	√	93.8	83.1	91.3	95.6	96.9	80.6	86.9	89.4	85.0	81.9	81.3	91.3	74.2	80.0	**86.5**	**6.5**

The best results are marked in bold. No TL represents a model with no transfer learning. * Reproduced.

TABLE II
RESULTS ON THE PHYSIONET DATASET

Method	Source-free	11	12	13	14	15	16	17	18	19	20	Mean	Std
No TL	√	71.4	75.0	78.6	75.0	92.9	60.7	67.9	85.7	92.9	64.3	76.4	10.6
DANN*	×	67.9	60.7	46.4	85.7	89.3	50.0	67.9	78.6	75.0	78.6	70.0	13.6
CDAN*	×	75.0	75.0	64.3	82.1	92.9	57.1	67.9	82.1	82.1	78.6	75.7	9.8
EA*	×	64.3	78.6	78.6	71.4	85.7	67.9	71.4	92.9	89.3	82.1	78.2	**9.0**
GSFDA*	√	71.4	78.6	78.6	71.4	96.4	60.7	67.9	82.1	85.7	75.0	76.8	9.5
NRC*	√	71.4	82.1	75.0	71.4	96.4	71.4	64.3	92.9	92.9	75.0	79.3	10.6
SHOT*	√	71.4	89.3	71.4	85.7	96.4	57.1	64.3	92.9	96.4	78.6	80.4	13.2
AEA-GSFDA	√	71.4	78.6	75.0	78.6	96.4	67.9	67.9	89.3	92.9	75.0	79.3	9.7
AEA-NRC	√	71.4	82.1	75.0	75.0	96.4	78.6	67.9	92.9	92.9	75.0	80.7	9.5
AEA-SHOT	√	71.4	85.7	75.0	82.1	96.4	71.4	67.9	92.9	92.9	78.6	**81.4**	9.7

The best results are marked in bold. No TL represents a model with no transfer learning. * Reproduced.

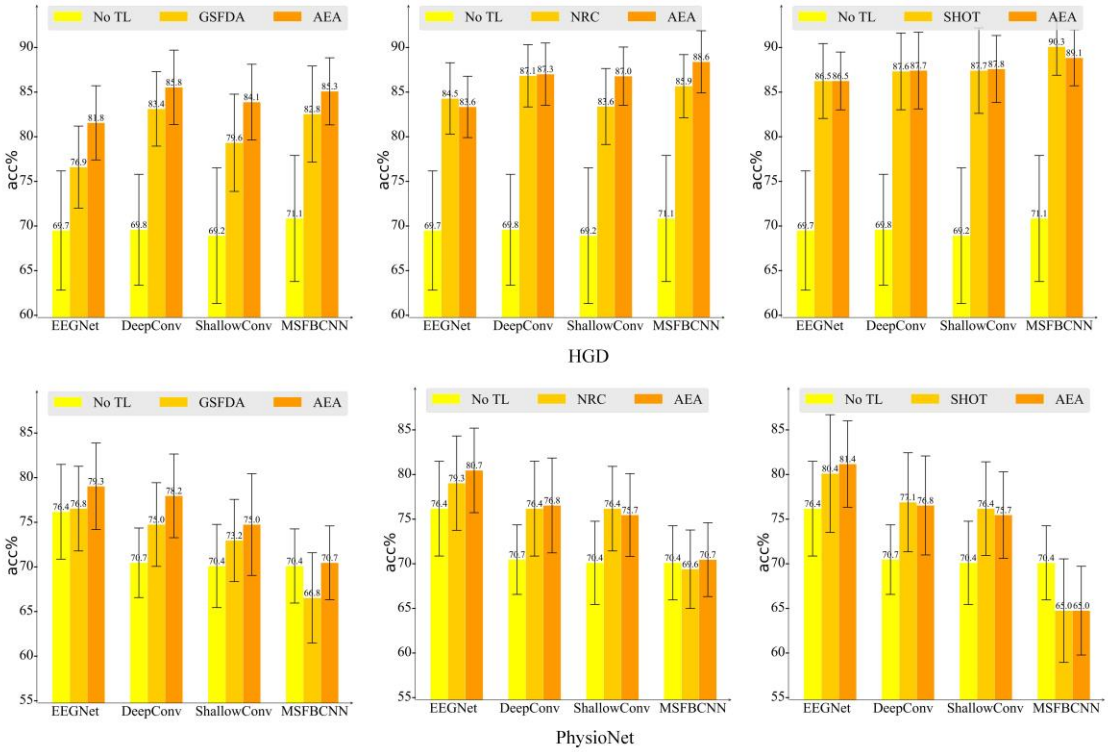

Fig. 3. Comparison of the average classification accuracies of the EEGNet, DeepConv, ShallowConv, and MSFBCNN models using the traditional SFDA methods and the AEA-based counterparts, respectively. The first and second rows show the results on the HGD and PhysioNet datasets, respectively.

To comprehensively analyze whether AEA-based SFDA methods can be the optimal choice in EEG source-free transfer learning tasks or, at the very least, serve as a viable alternative to traditional SFDA methods, we conducted comparisons across four widely used deep learning models, *i.e.*, EEGNet, DeepConv, ShallowConv, and MSFBCNN. The MI classification results on the HGD dataset are shown in Fig. 3. AEA-GSFDA significantly

This article has been accepted for publication in IEEE Journal of Biomedical and Health Informatics. This is the author's version which has not been fully edited and content may change prior to final publication. Citation information: DOI 10.1109/JBHI.2024.3463737

outperformed GSFDA, particularly on EEGNet, advancing the average accuracy from 76.9% to 81.8%. Next, AEA-NRC performed slightly worse than NRC on the EEGNet, with only a 0.9% difference in terms of accuracy. However, it outperformed NRC on the other models. Besides, AEA-SHOT and SHOT performed almost equally well on EEGNet, DeepConv, and ShallowConv, but it showed a 1.2% accuracy disadvantage on MSFBCNN. It could be attributed to the larger dataset size for HGD, allowing for more comprehensive training of the MSFBCNN model and alleviating the domain shift well. On the PhysioNet dataset, as shown in Fig. 3, AEA-GSFDA also significantly outperformed GSFDA, with the accuracies improved by at least 1.8% on the four models. Next, the accuracy of AEA-NRC is only 0.7% lower than that of NRC on ShallowConv, but it achieved the highest accuracy on the other models. Besides, AEA-SHOT and SHOT traded victories, but overall, AEA-SHOT got more gains, such as an increase of over 1% in accuracy on EEGNet. It is noteworthy that GSFDA, NRC, and SHOT on MSFBCNN performed poorly on the Physionet dataset. The number of model parameters is large and the PhysioNet dataset is small, which may make the transfer learning negative. Fortunately, AEA-GSFDAP and AEA-NRC do not suffer from negative transfer.

C. Classification Results on the ERP Dataset

We also used the EEGNet model for ERP classification tasks to evaluate three AEA-based SFDA methods on the P300 dataset. The ERP classification results of the AEA-based SFDA methods in comparison with related state-of-the-art methods, with or without a source-free condition, are presented in Table III. On the P300 dataset, the improvements brought by the tested methods are limited. However, AEA-SHOT and NRC achieved the greatest improvement compared to the model with no transfer learning. It is worth noting that the traditional EA suffers from negative transfer, but the AEA-based methods do not have this problem. It means that relying solely on alignment at the data level cannot address the domain drift in P300 data. However, the AEA algorithm utilizes adaptive adjustments from deep learning to make better data projections. Similarly, we comprehensively compared the traditional SFDA methods and their AEA-based counterparts using the EEGNet, DeepConv, ShallowConv, and MSFBCNN models. From Fig. 4, it can be observed that our proposed methods and traditional SFDA methods achieved comparable classification accuracies on the P300 dataset. The least favorable comparison result is from AEA-NRC on ShallowConv, which is 0.8% lower than NRC, while the most significant improvement comes from AEA-SHOT on ShallowConv, with a 1.2% increase over SHOT. Generally, the advantage of the AEA-based SFDA methods on the P300 dataset is not as great as on the MI datasets. The most likely reason is that the number of channels of the P300 dataset is only 8, and too few channels may be detrimental to learning the projection matrix.

TABLE III
RESULTS ON THE P300 DATASET

Method	Source-free	1	2	3	4	5	6	7	8	Mean	Std
No TL	√	62.1	51.8	61.4	67.7	61.8	61.8	65.4	62.1	61.8	4.3
DANN*	×	64.0	50.0	61.0	67.3	57.7	65.8	67.3	62.5	62.0	5.5
CDAN*	×	64.3	48.5	63.6	65.8	57.0	65.1	66.9	62.9	61.8	5.7
EA*	×	59.9	45.6	59.9	67.3	61.4	61.4	65.4	63.6	60.6	6.2
GSFDA*	√	63.6	50.0	61.8	69.1	62.1	63.6	67.3	63.2	62.6	5.3
NRC*	√	63.6	55.9	62.9	68.4	62.9	61.4	66.2	63.2	**63.1**	**3.4**
SHOT*	√	63.6	49.6	64.7	69.9	62.5	64.0	66.5	63.2	63.0	5.5
AEA-GSFDA	√	63.6	50.4	61.8	68.4	62.5	62.5	68.0	65.8	62.9	5.3
AEA-NRC	√	63.6	50.4	61.8	69.1	62.5	62.9	68.0	65.8	63.0	5.4
AEA-SHOT	√	63.6	52.2	61.8	68.0	62.9	62.9	68.0	65.8	**63.1**	4.7

The best results are marked in bold. No TL represents a model with no transfer learning. * Reproduced.

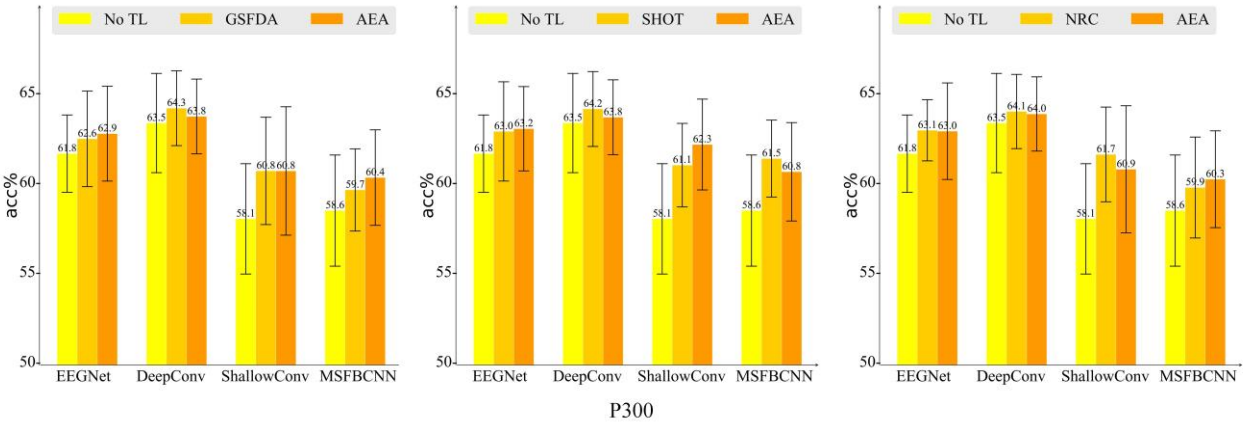

Fig. 4. Comparison of the average classification accuracies of the EEGNet, DeepConv, ShallowConv, and MSFBCNN models on the ERP dataset, using the traditional SFDA methods and the AEA-based counterparts, respectively.

D. Classification Results on the SSVEP Dataset

The results on the SSVEP dataset are shown in Table IV. On the SSVEP dataset, AEA-SHOT achieved lower

This article has been accepted for publication in IEEE Journal of Biomedical and Health Informatics. This is the author's version which has not been fully edited and content may change prior to final publication. Citation information: DOI 10.1109/JBHI.2024.3463737

accuracy than CDAN, but it still achieved the highest accuracy among SFDA methods. Most importantly, all three AEA-based methods outperformed their traditional SFDA counterparts. Additionally, EA again causes negative transfer, as seen in Table III. This may be because EA was originally used to transfer from a single source domain to a single target domain, while this study involves transferring from multiple source domains to a single target domain. Therefore, EA may have difficulty aligning accurately the covariance matrices of multiple source domains. Fig. 5 compares the results of traditional SFDA methods and their AEA-based counterparts using EEGNet, DeepConv, ShallowConv, and MSFBCNN models. It can be seen that AEA-GSFDA significantly outperformed GSFDA, particularly on the EEGNet model, where it achieved an 11.2% improvement in accuracy. Our method also exhibits superior classification accuracy compared to NRC and SHOT across EEGNet and DeepConv models. On ShallowConv and MSFBCNN models, the AEA-based methods achieved comparable classification results. Overall, the proposed AEA-based methods have demonstrated advanced performance on the SSVEP dataset.

TABLE IV
RESULTS ON THE SSVEP DATASET

Method	Source-free	26	27	28	29	30	31	32	33	34	35	Mean	Std
No TL	√	60	75	67.5	22.5	30	85	77.5	25	47.5	62.5	55.2	21.6
DANN*	×	72.5	100	70	22.5	60	85	92.5	30	60	85	67.8	24.2
CDAN*	×	82.5	97.5	77.5	30	62.5	90	92.5	32.5	70	87.5	**72.3**	22.8
EA*	×	57.5	72.5	62.5	17.5	37.5	80	72.5	35	32.5	50	51.8	19.6
GSFDA*	√	60	75	65	25	35	82.5	77.5	25	47.5	67.5	56	20.5
NRC*	√	65	95	72.5	25	45	95	95	27.5	52.5	80	65.2	25.6
SHOT*	√	60	77.5	80	25	35	90	77.5	25	55	72.5	59.8	22.7
AEA-GSFDA	√	82.5	77.5	77.5	27.5	55	85	80	32.5	77.5	77.5	67.2	20.2
AEA-NRC	√	80	80	80	25	55	85	77.5	42.5	62.5	77.5	66.5	**18.9**
AEA-SHOT	√	82.5	77.5	77.5	32.5	52.5	90	80	37.5	72.5	77.5	68	18.9

The best results are marked in bold. No TL represents a model with no transfer learning. * Reproduced.

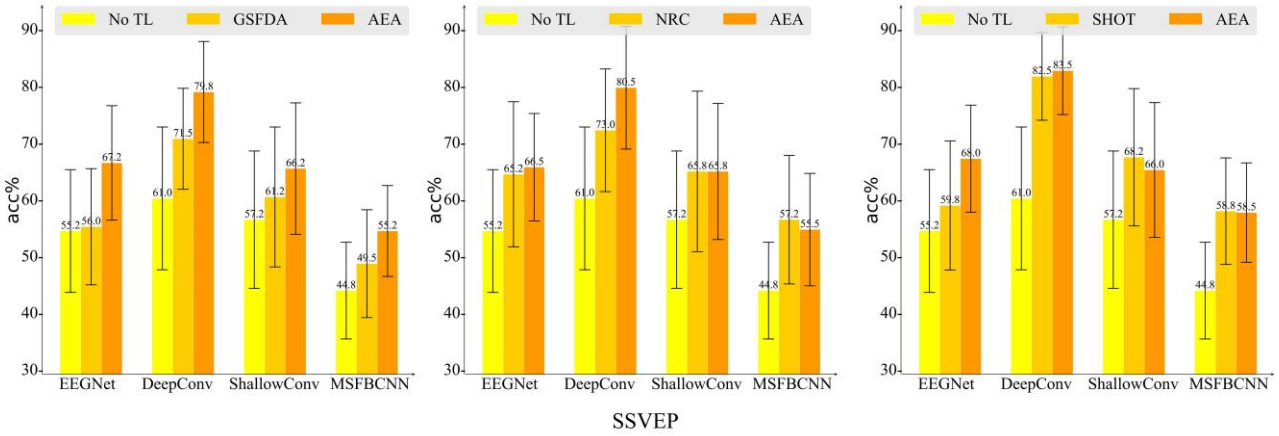

Fig. 5. Comparison of the average classification accuracies of the EEGNet, DeepConv, ShallowConv, and MSFBCNN models on the SSVEP dataset, using the traditional SFDA methods and the AEA-based counterparts, respectively.

E. Classification Results in Two Common Cases

Traditional domain adaptation ensures consistency in preprocessing between source and target data. However, in source-free domain adaptation, where source data is not visible, it cannot be guaranteed that the preprocessing of target data strictly matches that of source data. Consequently, some inconsistencies in preprocessing methods may further exacerbate domain drift issues. Thus, this paper studies two common cases in the EEG classification for subject-independent BCIs.

The first common case: The source domain is clean, while the target domain is noisy. We added Additive Gaussian White Noise (AGWN) with a mean of zero to the clean data of the target subject and obtained noisy EEG signals with a signal-to-noise ratio (SNR) of 10. Adding noise to data may further exacerbate the domain shift between the target and the source, which is a challenge for transfer learning. The classification results with noise added to the HGD dataset are presented in Table V. Comparing Table V and Table I, it is evident that the accuracy of each transfer learning method on the HGD dataset has decreased. However, our proposed methods consistently outperformed the respective non-AEA-based counterparts, improving accuracy by at least 2.1% in the three comparison groups. Table VI shows similar results on the PhysioNet dataset, and the average accuracies are advanced by our proposed methods from 78.6%, 78.6%, 80.7% to 79.6%, 80.4%, 82.5%, respectively. Table VII illustrates that adding noise to the P300 dataset also degrades the transfer effect, with the best-performing AEA-GSFDA only improving the accuracy by 0.8% compared to models without transfer learning. In this case, our proposed methods performed roughly on par with traditional SFDA methods. From Table VIII, it can be inferred that noise has the most significant impact on the performance on SSVEP dataset among the four datasets. The No TL approach achieved only 26% average accuracy. However, the AEA-based methods consistently outperformed the corresponding traditional SFDA methods under noisy conditions. Specifically, AEA-GSFDA

This article has been accepted for publication in IEEE Journal of Biomedical and Health Informatics. This is the author's version which has not been fully edited and content may change prior to final publication. Citation information: DOI 10.1109/JBHI.2024.3463737

achieved a remarkable 17.5% improvement compared to GSFDA, marking a significant advancement. In summary, the AEA-based SFDA methods are more robust in noisy environments. It could be attributed to the projection matrix being a global operation that captures stable relationships among channels.

The second common case: Many previous studies have improved the accuracy of pre-trained models by employing Euclidean alignment (EA) on multi-subject data in the source domain [19][20]. This alignment aims to equalize the average covariance matrices of all source subjects to the identity matrix. However, EA is not applied to the target domain. From Tables IX-XII, it is evident that the model with no transfer learning achieved notably low accuracy on each dataset. For instance, the accuracy on the HGD dataset dropped from 69.7% (as shown in Table I) to 45.7%, which indicates that the distribution disparity between the source domain with EA processing and the target domain without EA processing is exacerbated. Fortunately, our proposed methods can still alleviate the domain drift problem, which achieved the highest accuracy on the three datasets. From a group-level comparison perspective, except for AEA-GSFDA, which performed worse than GSFDA on the PhysioNet and P300 datasets in terms of accuracy, other AEA-based SFDA methods outperformed the non-AEA-based counterparts. The AEA-based SFDA methods performed better in this case because they rely on projection transformations, which align with the essence of EA, making it more effective in reducing domain drift.

TABLE V
RESULTS OF NOISY DATA IN HGD

Method	1	2	3	4	5	6	7	8	9	10	11	12	13	14	Mean	Std
No TL	88.1	66.9	73.1	88.8	72.5	63.8	77.4	68.1	69.4	41.3	71.9	84.4	47.2	62.5	69.7	13.1
GSFDA*	84.4	61.9	70.6	84.4	75.6	52.5	81.1	80.0	84.4	53.8	66.9	88.1	73.6	64.4	73.0	11.3
AEA-GSFDA	90.6	68.1	75.6	88.8	91.3	69.4	81.8	88.1	82.5	76.9	72.5	85.6	74.8	65.0	**79.4**	**8.5**
NRC*	91.9	73.1	85.0	88.8	91.3	73.8	84.9	87.5	87.5	63.1	75.6	91.9	78.6	68.1	81.5	9.1
AEA-NRC	90.0	78.8	85.0	93.8	91.3	75.6	84.9	88.8	82.5	81.3	75.6	90.6	79.3	73.8	**83.6**	**6.3**
SHOT*	82.5	81.3	86.3	85.6	93.8	73.1	83.0	95.0	83.8	78.8	76.3	87.5	72.3	81.9	82.9	6.4
AEA-SHOT	91.3	84.4	86.3	96.9	90.0	72.5	86.2	91.3	82.5	80.6	78.1	90.0	78.6	81.9	**85.0**	**6.3**

The best results for each comparison group are marked in bold. No TL represents a model with no transfer learning. * Reproduced.

TABLE VI
RESULTS OF NOISY DATA ON THE PHYSIONET DATASET

Method	11	12	13	14	15	16	17	18	19	20	Mean	Std
No TL	71.4	75.0	78.6	75.0	92.9	60.7	67.9	85.7	92.9	67.9	76.8	10.3
GSFDA*	71.4	82.1	78.6	75.0	96.4	75.0	57.1	85.7	92.9	71.4	78.6	10.8
AEA-GSFDA	71.4	82.1	78.6	71.4	96.4	78.6	67.9	85.7	92.9	71.4	**79.6**	**9.2**
NRC*	71.4	75.0	75.0	71.4	96.4	71.4	64.3	92.9	92.9	75.0	78.6	10.6
AEA-NRC	71.4	78.6	78.6	71.4	96.4	75.0	67.9	92.9	92.9	78.6	**80.4**	**9.6**
SHOT*	71.4	85.7	75.0	89.3	96.4	57.1	64.3	92.9	96.4	78.6	80.7	13.0
AEA-SHOT	75.0	85.7	78.6	85.7	96.4	71.4	67.9	92.9	96.4	75.0	**82.5**	**9.9**

The best results for each comparison group are marked in bold. No TL represents a model with no transfer learning. * Reproduced.

TABLE VII
RESULTS OF NOISY DATA ON THE P300 DATASET

Method	1	2	3	4	5	6	7	8	Mean	Std
No TL	59.9	48.9	62.5	68.0	61.8	61.4	66.5	61.8	61.4	5.4
GSFDA*	63.2	49.3	62.1	66.5	61.8	62.5	67.7	61.0	61.8	5.2
AEA-GSFDA	61.0	50.4	61.4	68.0	62.1	62.1	65.8	66.9	**62.2**	**5.1**
NRC*	58.8	55.2	61.8	66.9	62.1	63.6	65.8	62.1	**62.0**	**3.5**
AEA-NRC	61.4	50.4	61.4	65.4	62.1	61.8	65.1	66.5	61.8	4.7
SHOT*	62.9	49.6	64.3	67.3	62.5	62.9	65.8	61.0	62.0	**5**
AEA-SHOT	60.7	50.4	61.4	68.0	62.1	62.5	65.1	66.5	**62.1**	5.1

The best results for each comparison group are marked in bold. No TL represents a model with no transfer learning. * Reproduced.

TABLE VIII
RESULTS OF NOISY DATA ON THE SSVEP DATASET

Method	26	27	28	29	30	31	32	33	34	35	Mean	Std
No TL	20	45	30	0	22.5	37.5	40	15	25	25	26	12.5
GSFDA*	25	47.5	35	12.5	17.5	42.5	40	15	35	27.5	29.8	11.5
AEA-GSFDA	50	60	72.5	15	37.5	60	62.5	15	42.5	57.5	**47.3**	18.7
NRC*	37.5	65	45	12.5	22.5	52.5	52.5	17.5	35	35	37.5	15.9
AEA-NRC	50	55	65	15	30	57.5	62.5	15	32.5	60	**44.3**	18.4
SHOT*	47.5	57.5	67.5	12.5	20	77.5	65	17.5	37.5	45	44.8	21.5
AEA-SHOT	52.5	60	72.5	15	32.5	65	62.5	17.5	42.5	57.5	**47.8**	19.1

The best results for each comparison group are marked in bold. No TL represents a model with no transfer learning. * Reproduced.

This article has been accepted for publication in IEEE Journal of Biomedical and Health Informatics. This is the author's version which has not been fully edited and content may change prior to final publication. Citation information: DOI 10.1109/JBHI.2024.3463737

TABLE IX
RESULTS OF EUCLIDEAN-ALIGNED DATA ON THE HGD DATASET

Method	1	2	3	4	5	6	7	8	9	10	11	12	13	14	Mean	Std
No TL	49.4	28.1	37.5	47.5	44.4	32.5	49.7	40.0	41.3	40.0	58.8	66.9	54.1	49.4	45.7	9.9
GSFDA*	67.5	79.4	72.5	83.8	79.4	34.4	62.9	65.0	63.8	74.4	68.8	88.8	65.4	48.8	68.2	13.5
AEA-GSFDA	81.9	79.4	81.9	77.5	88.8	60.0	66.0	83.1	80.6	78.1	71.3	81.3	78.6	56.3	**76.1**	**9.0**
NRC*	82.5	81.3	75.6	91.9	86.3	51.9	62.9	76.9	81.9	83.1	73.8	77.5	78.0	56.9	75.7	10.8
AEA-NRC	96.3	93.1	87.5	95.0	91.3	66.9	73.0	86.9	88.8	85.0	71.9	85.6	83.0	65.6	**83.6**	**9.8**
SHOT*	92.5	85.6	86.3	98.1	91.3	73.1	74.2	86.3	88.1	84.4	74.4	92.5	69.8	63.1	82.8	**9.8**
AEA-SHOT	94.4	88.8	88.1	96.9	96.9	68.1	71.7	91.3	92.5	82.5	81.9	84.4	78.6	65.6	**84.4**	9.9

The best results for each comparison group are marked in bold. No TL represents a model with no transfer learning. * Reproduced.

TABLE X
RESULTS OF EUCLIDEAN-ALIGNED DATA ON THE PHYSIONET DATASET

Method	11	12	13	14	15	16	17	18	19	20	Mean	Std
No TL	53.6	25.0	53.6	42.9	67.9	39.3	39.3	78.6	53.6	67.9	52.1	15.3
GSFDA*	78.6	64.3	60.7	57.1	60.7	78.6	60.7	78.6	57.1	67.9	**66.4**	**8.5**
AEA-GSFDA	64.3	64.3	60.7	46.4	71.4	60.7	42.9	71.4	53.6	71.4	60.7	9.7
NRC*	60.7	64.3	67.9	60.7	60.7	64.3	42.9	82.1	71.4	71.4	64.6	**9.6**
AEA-NRC	71.4	75.0	64.3	71.4	67.9	64.3	42.9	82.1	71.4	60.7	**67.1**	10.0
SHOT*	64.3	67.9	67.9	53.6	75.0	67.9	53.6	89.3	64.3	67.9	67.1	**9.7**
AEA-SHOT	64.3	71.4	75.0	57.1	78.6	75.0	46.4	78.6	71.4	67.9	**68.6**	**9.7**

The best results for each comparison group are marked in bold. No TL represents a model with no transfer learning. * Reproduced.

TABLE XI
RESULTS OF EUCLIDEAN-ALIGNED DATA ON THE P300 DATASET

Method	1	2	3	4	5	6	7	8	Mean	Std
No TL	59.6	46.0	67.3	56.6	48.9	55.9	58.8	61.4	56.8	6.4
GSFDA*	64.0	50.0	66.9	62.1	55.5	64.3	57.4	65.1	**60.7**	**5.4**
AEA-GSFDA	61.8	46.3	66.9	65.8	59.6	61.0	60.7	59.9	60.3	5.8
NRC*	62.9	48.9	67.7	67.3	51.1	65.8	58.1	60.3	60.3	6.7
AEA-NRC	63.6	46.7	66.9	65.4	59.2	61.8	62.9	62.9	**61.2**	**5.9**
SHOT*	60.7	46.0	67.3	60.3	53.3	63.6	57.0	59.9	58.5	6.1
AEA-SHOT	62.1	47.1	66.9	65.4	59.2	61.0	62.9	59.2	**60.5**	**5.7**

The best results for each comparison group are marked in bold. No TL represents a model with no transfer learning. * Reproduced.

TABLE XII
RESULTS OF EUCLIDEAN-ALIGNED DATA ON THE SSVEP DATASET

Method	26	27	28	29	30	31	32	33	34	35	Mean	Std
No TL	27.5	30	27.5	5	22.5	10	27.5	7.5	10	27.5	19.5	**9.5**
GSFDA*	40	50	37.5	15	22.5	32.5	42.5	15	20	50	32.5	12.9
AEA-GSFDA	45	72.5	67.5	15	52.5	77.5	72.5	40	55	60	**55.8**	17.7
NRC*	50	52.5	40	15	32.5	47.5	57.5	17.5	22.5	65	40	16.6
AEA-NRC	42.5	75	67.5	15	32.5	75	55	25	57.5	62.5	**50.8**	20
SHOT*	45	72.5	45	17.5	27.5	62.5	50	17.5	22.5	62.5	42.3	19.1
AEA-SHOT	45	75	70	12.5	32.5	72.5	72.5	37.5	55	62.5	**53.5**	20.0

The best results for each comparison group are marked in bold. No TL represents a model with no transfer learning. * Reproduced.

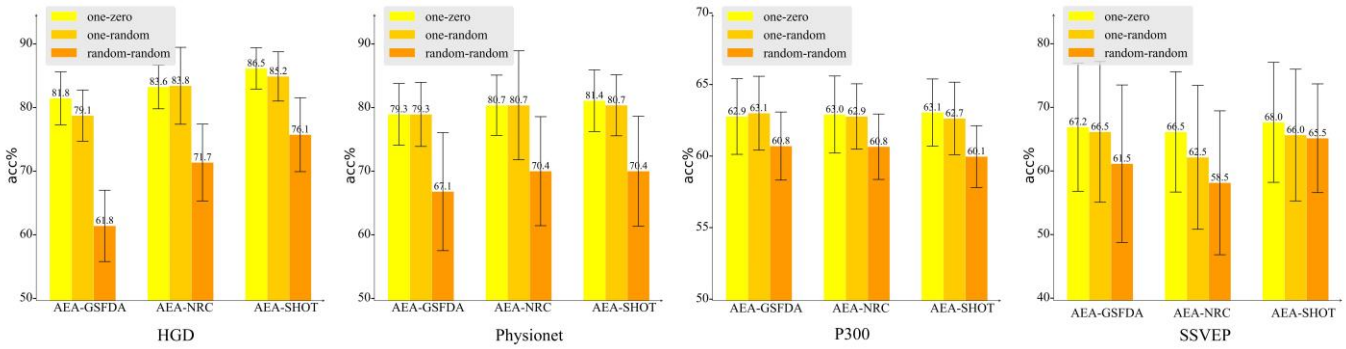

Fig. 6. Comparison of the average classification accuracies of the AEA-based SFDA methods with different ways for initialization of *P*. "one-zero" represents that the diagonal elements are initialized to 1, and the other elements are initialized to 0. "one-random" represents that the diagonal elements as initialized to 1, while the other elements are randomly initialized, as shown in eq. (12). "random-random" represents that all elements are randomly initialized.

This article has been accepted for publication in IEEE Journal of Biomedical and Health Informatics. This is the author's version which has not been fully edited and content may change prior to final publication. Citation information: DOI 10.1109/JBHI.2024.3463737

F. Different Ways for Initializing P

A reasonable initialization of the projection matrix is crucial for achieving good performance. Fig. 6 illustrates the impact of three initialization methods on the performance of AEA-GSFDA, AEA-NRC, and AEA-SHOT. The "one-zero" initialization corresponds to an identity matrix and achieved the best overall classification performance. The "one-random" initialization performed slightly worse than "one-zero" initialization on average but surpassed "one-zero" for AEA-NRC on the HGD dataset. The poorest results are obtained from "random-random" initialization. Based on these results, it becomes clear that setting the diagonal elements of the projection matrix to one is of utmost importance, as it ensures that the projection matrix, during its initial training, does not transform the original data drastically.

G. Visualization

Each AEA-based SFDA method effectively reduces the distribution discrepancy between the target and source domains, improving the accuracy of the pre-trained model on the target domain. To illustrate the distribution effect of EEG features before and after using the AEA-based SFDA methods, Fig. 7, taking AEA-SHOT as an example, visualizes the data distribution with the aid of t-distributed stochastic neighbor embedding (T-SNE) [55].

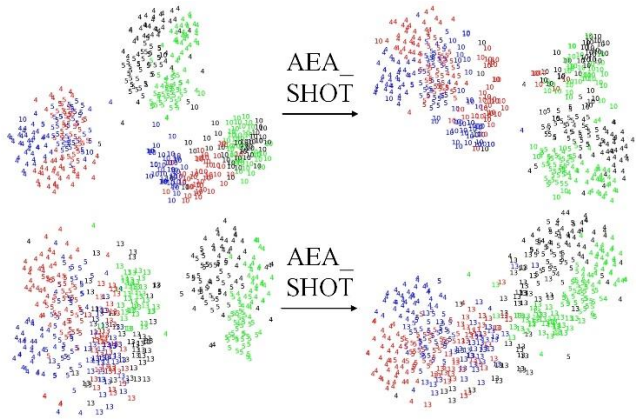

Fig. 7. T-SNE maps for feature vectors from the last convolutional layer of the EEGNet on the HGD dataset. The numbers and colors represent subjects and categories, respectively, where "4" and "5" represent source subjects, while "10" and "13" represent target subjects. The target subjects in the left column have not been transferred, while the target objects in the right column have been transferred by AEA-SHOT. All data are from test sets.

It can be observed from the left column that the distributions of source subjects 4 and 5 are overlapped, and they form clusters in terms of categories (MI tasks). However, target subjects 10 and 13 distributions are almost linearly separable from source subjects 4 and 5. From a category-level perspective, some categories of subjects 10 and 13 are clustered together and distinguishable from other categories. It is attributed to the powerful feature extraction capabilities of the pre-trained model, which reduce the spatial distance between features belonging to the same category. Nonetheless, it is difficult for the classifier trained by the data of source subjects to classify the data of target subjects accurately. AEA-SHOT utilizes only a projection matrix to transform the EEG data of target subjects into data that the pre-trained model is "familiar with," thus harnessing its robust classification ability developed in the source domain. As evident from the figures in the right column, AEA-SHOT makes target subjects and source subjects closer, thereby reducing domain drift.

TABLE XIII
THE NUMBER OF TRAINABLE WEIGHTS FOR A TRANSFER PROCESS

Dataset	EEG-Net	Deep-Conv	Shallow-Conv	MSFB-CNN	AEA-based
HGD	14.3k	297.5k	82.5k	299k	990
PhysioNet	13.8k	305.2k	109.4k	421.7k	2080
P300	8.2k	270.6k	18.1k	61.9k	36
BenchMark	22.3k	325.3k	102.4k	169.9k	115

TABLE XIV
THE PERCENTAGE INCREASE IN FLOPS OF THE PROJECTION MATRIX ACROSS DIFFERENT DATASETS AND MODELS

Dataset	EEGNet	Deep-Conv	Shallow-Conv	MSFBCNN
HGD	4.9%	8.5%	2.0%	0.8%
PhysioNet	6.1%	12%	5.1%	1.0%
P300	0.7%	0.4%	0.6%	0.1%
BenchMark	0.5%	0.8%	0.8%	0.1%

TABLE XV
THE INFERENCE TIME FOR 10 RANDOMLY SELECTED SUBJECTS ON HGD DATASET (UNIT: MS)

Dataset	EEGNet	Deep-Conv	Shallow-Conv	MSFBCNN
SHOT	26.5	7.3	14.6	19.12
AEA-SHOT	3	1.1	1.82	2

There is only one sample from each subject.

H. Lightweight

Table XIII shows that our method has significantly fewer trainable weights than other methods. Table XIV shows that the additional FLOPs introduced by the projection matrix is no more than 12%, and in some cases, only 0.1%. However, the advantage of the AEA-based methods lies in multi-subject inference. Table XV demonstrates that our method can greatly reduce the inference time for multi-subject inference, as shown by the comparison results of SHOT and AEA-SHOT.

V. DISCUSSIONS

The mainstream domain adaptation methods align the distributions of two domains in the feature space, allowing for end-to-end training of models with the convenience and efficiency of deep learning. However, the cumbersome approach of "updating a deep learning model for each new subject" in the EEG field can be further optimized. For instance, methods like covariance matrix alignment [34][35], handling domain shifts on raw data, or manual features are independent of models. However, these methods may sacrifice the advantage of end-to-end deep learning training. Therefore, "end-to-end learning" and "avoid updating models" may seem contradictory. The AEA algorithm proposed in this paper solves the issues mentioned above together. We embed a projection matrix between the target data and the pre-trained model. Consequently, we can still train this projection matrix end-to-end while freezing the pre-trained model weights. Furthermore, we utilize existing SFDA algorithms without the need for source data.

A. Statistical Analysis and Discussion

What we need to be concerned about is whether the accuracy of the AEA-based SFDA methods is affected compared to traditional SFDA methods that require updating model weights. Relevant experimental results demonstrate that the accuracy of AEA remains

state-of-the-art (as shown in Tables I-IV). Following the conventions in previous EEG studies [53][54], a Wilcoxon signed-rank test is used to evaluate our proposed methods further. The calculation of statistical significance between the AEA-based SFDA methods and non-AEA-based counterparts on each dataset is based on accuracy data (as shown in Figs. 3 - 5) for all models *(i.e.*, EEGNet, Shallow ConvNet, Deep ConvNet, and MSFBCNN) across subjects. P-values are obtained via the one-tailed Wilcoxon signed-rank test of accuracy, whose null hypothesis is that the performance of AEA-based SFDA methods is better than non-AEA-based counterparts. The statistical test results are shown in Table XVI, with significant results (p-value < 0.05) highlighted in bold. The p-values inside parentheses are obtained via the two-tailed Wilcoxon signed-rank test of accuracy, whose null hypothesis is that there is a significant difference in classification accuracy between the AEA-based SFDA methods and non-AEA-based counterparts. The results inside parentheses that do not show a significant difference (p-value > 0.05) are highlighted with a gray background. From Table XVI, it is evident that AEA-GSFDA significantly outperformed GSFDA on the MI and SSVEP datasets. AEA-NRC also demonstrated its superiority on the HGD dataset. Except for the above cases, there is no significant difference in classification accuracy between the AEA-based SFDA methods and their non-AEA-based counterparts. It implies that our proposed methods can at least be an alternative to traditional SFDA methods and may even outperform them with higher efficiency.

TABLE XVI
P-VALUES

Dataset	AEA-GSFDA	AEA-NRC	AEA-SHOT
HGD	**<0.001**	**0.015**	0.76(0.4757)
PhysioNet	**<0.001**	0.11(0.221)	0.83(0.343)
P300	0.16(0.325)	0.30(0.592)	0.42(0.84)
BenchMark	**<0.001**	0.16(0.32)	0.24(0.48)

Our proposed projection matrix learning differs from fine-tuning model parameters in that it aims to maintain the model's performance in the source domain. Models trained in the source domain typically perform optimally only within that domain. Fine-tuning pre-trained models can lead to a decline in classification performance in the source domain. Additionally, the absence of labels makes it challenging to achieve optimal performance in the target domain. In contrast, our projection matrix transforms target domain data into source domain data, which can be processed by pre-trained models. This allows us to fully leverage the pre-trained model's optimal feature extraction capabilities in the source domain. Results show that our method significantly outperformed the corresponding SFDA methods. Furthermore, the GSFDA method generally performed weaker than NRC and SHOT in our experiments. Apart from the P300 dataset, the advantages of AEA-GSFDA over GSFDA are statistically significant on other datasets, and the results are comparable to those of AEA-NRC and AEA-SHOT. Fine-tuning the model to achieve optimal performance in the target domain is more challenging for GSFDA. However, our method can significantly alleviate this issue, indicating that it can improve methods that initially exhibit poor performance.

B. Discussion on the Effectiveness of AEA in Data Transfer

AEA can effectively transform target domain data into source domain data because of EA and adaptation.

EA [24] aims to equate the covariance matrices of two domains. The off-diagonal elements of the covariance matrix calculated in this paper represent the linear relationships between channels (*i.e.*, electrodes), whilst the diagonal elements correspond to the magnitude of signals on channels. From a biological perspective, channels represent brain regions. Differences exist in the EEGs elicited by the same brain region across different subjects, as well as variations in the correlations between brain regions, directly causing differences in the distributions of EEG data among subjects. When the relationships between EEG channels and the magnitudes of signals are consistent between two subjects, the distribution differences in data are eliminated, thus enhancing transferability.

Adaptation enables EA to be data-driven and learn the appropriate projection matrix end-to-end. We further illustrate adaptability by comparing it with graph embeddings. Graph embedding of EEG signals also conforms to eq. (5) [56][57]. A relationship exists between the projection described by eq. (5) and the adjacency matrix used in graph embedding. The construction of the adjacency matrix is usually based on the physical locations of electrodes or the correlation of EEG signals, which determines the strength and connectivity of information transfer between channels, simulating the connectivity between brain regions. On the other hand, the projection matrix in this paper is designed to align the EEG signals in the target domain, ensuring that the relationships between channels in the target domain match those in the source domain. However, the adaptation of AEA allows the projection matrix to achieve alignment and play a role in uncovering channel connectivity. It explains why the AEA's projection matrix outperformed the traditional EA's projection matrix in our experiments. Therefore, it can be said that AEA combines both "domain adaptation" and "graph embedding." The advantage of graph embedding lies in its structural stability. Specifically, the stable relationships between channels mitigate the interference from noisy signals to some extent (as seen in Tables V-VIII).

C. Discussion on the Advantages of AEA in Global Transformations

This paper also considers scenarios where source and target domain data processing is not strictly consistent: whether the data contains noise and whether the data has EA preprocessing. These two scenarios exacerbate distribution differences between the source and target domains. Fortunately, AEA is better at mitigating these adverse effects compared to other methods. Unlike convolutional networks, which excel at local processing, AEA handles global relationships better because it can perform global transformations on the data. Noise and EA preprocessing alter inter-channel relationships, and AEA is inherently good at altering these relationships to restore the data to a distribution familiar to the model. Therefore, AEA is more effective than other transfer learning methods in handling changes in data channel relationships.

D. Discussion on Lightweight Application Scenarios of AEA

The most important advantage of our proposed methods is their lightweight nature, primarily reflected in the small number of trainable weights. Traditional SFDA methods necessitate a separate updating model for each subject. As new subjects are added, the required storage space for trainable weights can grow significantly. In contrast, AEA only requires learning a projection matrix for each new subject without altering the weights of the pre-trained model, leading to a substantial reduction in storage space needed for trainable weights. For example, on the P300 dataset, the number of trainable weights in AEA-based DeepConv is only approximately $1/7517$ of that in DeepConv without AEA-based transfer (as shown in Table XIII), and competitive performance is obtained without updating the pre-trained model (as shown in Fig. 4). AEA slightly increases runtime for single-subject inference, as shown by the increase in Floating Point Operations (FLOPs) in Table XIV. However, AEA's time advantage becomes significant during multi-subject inference. This is because multiple subjects can be inferred using the same deep model, rather than requiring a separate model for each subject. Traditional transfer learning methods may need to load different models to infer different subjects sequentially, whereas AEA loads a single model to infer multiple subjects in parallel (as shown in Table XV).

Currently, GPT-like large language models have been widely adopted, driving research on EEG-based large models [58]. AEA shows great potential for application in large models. An example of using BCIs to control mouse movement in a cloud-local deployment scenario is shown in Fig. 8. Locally, only a projection matrix is required to transfer the local user's EEG data, while a large model deployed on the cloud performs parallel inference on multi-user data and returns the inference results to the local device. Local BCIs can control mouse movements based on the returned instructions.

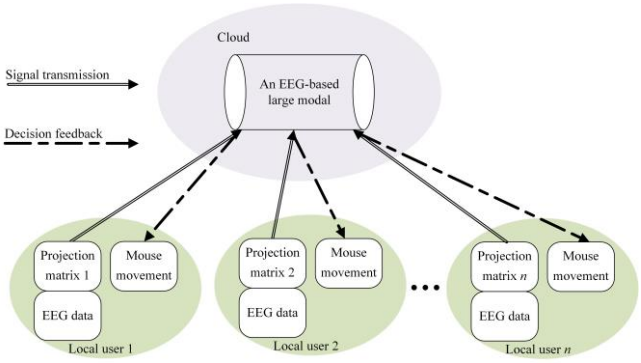

Fig. 8. A cloud-local deployment scenario for mouse movement control based on AEA-BCIs.

E. Future Work

There are two possible directions for future work:

1) Cross-dataset recognition, such as transferring from HGD to the PhysioNet datasets. Due to the variation in the number of EEG channels, the format of the projection matrix would also need to be adjusted. Further research is required to investigate whether the AEA algorithm remains effective.
2) Cross-task recognition. Label alignment (LA) enables EA to be applicable for cross-task recognition [36]. Therefore, AEA should also have the potential for cross-task recognition.

VI. Conclusion

This paper proposes novel source-free domain adaptation methods for EEG classification based on adaptive Euclidean alignment to avoid updating pre-trained deep learning models for subject-independent BCIs to handle new target subjects. Our methods only require learning a single projection matrix to align the distribution of the target domain with the source domain without the need of updating pre-trained deep learning models. The proposed methods enhanced the efficiency and the EEG classification performance of four widely used EEG deep learning models on two public MI datasets, one ERP dataset and one SSVEP dataset. Furthermore, our methods achieved superior EEG classification performance when applied to the target domain data without denoising and EA alignment, demonstrating highly adaptive capability in handling inconsistent data processing between the source and target domains.

References

[1] R. Janapati, et al., "Advances in modern EEG-BCI signal processing: A review, " *Materials Today: Proceedings*, vol. 80, pp. 2563-2566, 2023.
[2] X. Xiong, et al., "Weighted brain network metrics for decoding action intention understanding based on EEG, " *Frontiers in Human Neuroscience*, vol. 14, p. 232, 2020.
[3] X. Yin, et al., "Optimal channel-based sparse time-frequency blocks common spatial pattern feature extraction method for motor imagery classification," *Mathematical Biosciences and Engineering*, vol. 18, no. 4, pp. 4247-4263, 2021.
[4] L. Gu, et al., "EEG-based classification of lower limb motor imagery with brain network analysis," *Neuroscience*, vol. 436, pp. 93-109, 2020
[5] E.S. Kappenman, et al., "ERP CORE: An open resource for human event-related potential research," *NeuroImage*, vol. 225, p. 117465, 2021
[6] M. Gongora, et al., "Event-related potential (P300): the effects of levetiracetam in cognitive performance," *Neurological Sciences*, vol. 42, pp. 2309-2316, 2021.
[7] B. Liu, et al., "BETA: A large benchmark database toward SSVEP-BCI application," *Frontiers in Neuroscience*, vol. 14, p. 627, 2020.
[8] Y. Chen, et al., "A novel training-free recognition method for SSVEP-based BCIs using dynamic window strategy," *Journal of Neural Engineering*, vol. 18, no. 3, p. 036007, 2021.
[9] M. Rashed-Al-Mahfuz, et al., "A deep convolutional neural network method to detect seizures and characteristic frequencies using epileptic electroencephalogram (EEG) data," *IEEE Journal of Translational Engineering in Health and Medicine*, vol. 9, pp. 1-12, 2021
[10] A. Shoeibi, et al., "A comprehensive comparison of handcrafted features and convolutional autoencoders for epileptic seizures detection in EEG signals," *Expert Systems with Applications*, vol. 163, p. 113788, 2021.
[11] X. Gu, et al., "EEG-based brain-computer interfaces (BCIs): A survey of recent studies on signal sensing technologies and computational intelligence approaches and their applications," *IEEE/ACM Transactions on Computational Biology and Bioinformatics*, vol. 18, no. 5, pp. 1645-1666, 2021.
[12] X. Liu, et al., "Multiscale space-time-frequency feature-guided multitask learning CNN for motor imagery EEG classification," *Journal of Neural Engineering*, vol. 18, no. 2, p. 026003, 2021.
[13] Y. Hou, et al., "GCNs-net: A graph convolutional neural network approach for decoding time-resolved EEG motor imagery signals," *IEEE Transactions on Neural Networks and Learning Systems*, 2022.
[14] Q. She, et al., "Multi-source manifold feature transfer learning with domain selection for brain-computer interfaces," *Neurocomputing*, vol. 514, pp. 313-327, 2022.
[15] D. Wu, et al., "Transfer learning for EEG-based brain–computer interfaces: A review of progress made since 2016," *IEEE Transactions on Cognitive and Developmental Systems*, vol. 14, no. 1, pp. 4-19, 2020.

[16] Y. Ganin and V. Lempitsky, "Unsupervised domain adaptation by backpropagation," In *International Conference on Machine Learning*, 2015, pp. 1180-1189.
[17] M. Long, et al., "Conditional adversarial domain adaptation," In *Advances in Neural Information Processing Systems*, vol. 31, 2018
[18] B. Sun and K. Saenko, "Deep coral: Correlation alignment for deep domain adaptation," In *Computer Vision–ECCV*, 2016, pp. 443-450.
[19] W. Zhang and D. Wu, "Manifold embedded knowledge transfer for brain-computer interfaces," *IEEE Transactions on Neural Systems and Rehabilitation Engineering*, vol. 28, no. 5, pp.1117-1127, 2020.
[20] Y. Gao, et al., "Double stage transfer learning for brain–computer interfaces," *IEEE Transactions on Neural Systems and Rehabilitation Engineering*, vol. 31, pp. 1128-1136, 2023.
[21] N. Ding, et al., "Source-free domain adaptation via distribution estimation," In *Proceedings of the IEEE/CVF Conference on Computer Vision and Pattern Recognition*, 2022, pp. 7212-7222.
[22] L. Yi, et al., "When source-free domain adaptation meets learning with noisy labels," *arXiv preprint arXiv:2301.13381*, 2023.
[23] J. Liang, et al., "Do we really need to access the source data? source hypothesis transfer for unsupervised domain adaptation," In *International Conference on Machine Learning*, 2020, pp. 6028-6039.
[24] H. He and D. Wu, "Transfer learning for brain–computer interfaces: A Euclidean space data alignment approach," *IEEE Transactions on Biomedical Engineering*, vol. 67, no. 2, pp. 399-410, 2019.
[25] S. Yang, et al., "Generalized source-free domain adaptation," In *Proceedings of the IEEE/CVF International Conference on Computer Vision*, 2021, pp. 8978-8987,
[26] S. Yang, et al., "Exploiting the intrinsic neighborhood structure for source-free domain adaptation," In *Advances in Neural Information Processing Systems*, vol. 34, pp. 29393-29405, 2021.
[27] S. Yang, et al., "Unsupervised domain adaptation without source data by casting a bait," *arXiv preprint arXiv:2010.12427*, vol 1, no. 2, p. 5, 2020
[28] H. Xia, et al., "Adaptive adversarial network for source-free domain adaptation," In *Proceedings of the IEEE/CVF International Conference on Computer Vision*, 2021, pp. 9010-9019.
[29] R. Li, et al., "Model adaptation: Unsupervised domain adaptation without source data," In *Proceedings of the IEEE/CVF Conference on Computer Vision and Pattern Recognition*, 2020, pp. 9641-9650.
[30] V. K. Kurmi, et al., "Domain impression: a source data free domain adaptation method," In *2021 IEEE Winter Conference on Applications of Computer Vision*, 2021, pp. 615-625.
[31] O.B. Guney, et al., "Source free domain adaptation of a DNN for SSVEP-based brain-computer interfaces," *arXiv preprint arXiv:2305.17403*, 2023.
[32] K. Xia, et al., "Privacy-preserving domain adaptation for motor imagery-based brain-computer interfaces," *IEEE Transactions on Biomedical Engineering*, vol. 69, no. 11, pp. 3365-3376, 2022.
[33] C. Zhao et al., "Source-free domain adaptation (SFDA) for privacy-preserving seizure subtype classification," *IEEE Transactions on Neural Systems and Rehabilitation Engineering*, vol. 31, pp. 2315-2325, 2023.
[34] P. Zanini, et al., "Transfer learning: A Riemannian geometry framework with applications to brain–computer interfaces," *IEEE Transactions on Biomedical Engineering*, vol. 65, no. 5, pp. 1107-1116, 2017.
[35] R.C. Maswanganyi, et al., "Multi-class transfer learning and domain selection for cross-subject EEG classification," *Applied Sciences*, vol. 13, no. 8, p. 5205, 2023.
[36] H. He and D. Wu, "Different set domain adaptation for brain-computer interfaces: a label alignment approach," *IEEE Transactions on Neural Systems and Rehabilitation Engineering*, vol. 28, no. 5, pp. 1091-1108, 2020.
[37] M. Dai, et al., "Transfer kernel common spatial patterns for motor imagery brain-computer interface classification," *Computational and Mathematical Methods in Medicine*, vol. 2018, p. 9871603, 2018.
[38] H. Albalawi and X. Song, "A study of kernel CSP-based motor imagery brain computer interface classification," In *2012 IEEE Signal Processing in Medicine and Biology Symposium*, 2021, pp. 1-4.
[39] M. Long, et al., "Domain invariant transfer kernel learning," *IEEE Transactions on Knowledge and Data Engineering*, vol. 27, no. 6, pp. 1519-1532, 2014.
[40] Z. Lan, Z., et al., "Domain adaptation techniques for EEG-based emotion recognition: a comparative study on two public datasets," *IEEE Transactions on Cognitive and Developmental Systems*, vol. 11, no. 1, pp. 85-94, 2018.
[41] S. J. Pan, et al., "Domain adaptation via transfer component analysis," *IEEE Transactions on Neural Networks*, vol. 22, no. 2, pp. 199-210, 2010.
[42] Y. Zhang, et al, "Seizure classification from EEG signals using an online selective transfer TSK fuzzy classifier with joint distribution adaption and manifold regularization," *Frontiers in Neuroscience*, vol. 14, p. 496, 2020.
[43] M. Long, et al. "Transfer feature learning with joint distribution adaptation," In *Proceedings of the IEEE International Conference on Computer Vision*, 2013, pp. 2200-2207.
[44] L. Zhu, et al, "Multi-source fusion domain adaptation using resting-state knowledge for motor imagery classification tasks," *IEEE Sensors Journal*, vol. 21, no. 19, pp. 21772-21781, 2021.
[45] J. Wang, et al., "Balanced distribution adaptation for transfer learning," In *2017 IEEE International Conference on Data Mining*, 2021, pp. 1129-1134.
[46] K. Guan, K., et al., "Cross-task mental workload recognition based on EEG tensor representation and transfer learning," *IEEE Transactions on Neural Systems and Rehabilitation Engineering*, vol. 31, 2023.
[47] D. Tao, et al., "General tensor discriminant analysis and gabor features for gait recognition," *IEEE Transactions on Pattern Analysis and Machine Intelligence*, vol. 29, no. 10, pp. 1700-1715, 2017.
[48] R.T. Schirrmeister, et al., "Deep learning with convolutional neural networks for EEG decoding and visualization," *Human brain mapping*, vol. 38, no. 11, pp. 5391-5420, 2017.
[49] A.L. Goldberger, et al., "PhysioBank, PhysioToolkit, and PhysioNet: components of a new research resource for complex physiologic signals," *Circulation*, vol. 101, no. 23, pp. e215-e220, 2000.
[50] Y. Wang, et al., "A benchmark dataset for SSVEP-based brain–computer interfaces," *IEEE Transactions on Neural Systems and Rehabilitation Engineering*, vol. 25, no. 10, pp. 1746-1752, 2016.
[51] V.J. Lawhern, et al., "EEGNet: a compact convolutional neural network for EEG-based brain–computer interfaces. *Journal of Neural Engineering*, vol. 15 no. 5, p. 056013, 2018.
[52] H. Wu, et al., "A parallel multiscale filter bank convolutional neural networks for motor imagery EEG classification," *Frontiers in Neuroscience*, vol. 13, p. 1275, 2019.
[53] H. Wang, et al., "Motor imagery EEG classification based on a weighted multi-branch structure suitable for multisubject data," *IEEE Transactions on Biomedical Engineering*, vol. 70, no. 11, pp. 3040-3051, 2023.
[54] M. Li and W. Chen, "FFT-based deep feature learning method for EEG classification," *Biomedical Signal Processing and Control*, vol. 66, p.102492, 2021.
[55] L. Van der Maaten and G. Hinton, "Visualizing data using t-SNE," *Journal of Machine Learning Research*, vol. 9, no. 11, 2008.
[56] D. Zhang, et al., "Motor imagery classification via temporal attention cues of graph embedded EEG signals," *IEEE Journal of Biomedical and Health Informatics*, vol. 24, no. 9, pp. 2570-2579, 2020.
[57] P. Zhong, et al., "EEG-based emotion recognition using regularized graph neural networks," *IEEE Transactions on Affective Computing*, vol. 13, no. 3, pp.1290-1301, 2020.
[58] W. B. Jiang, et al., "Large brain model for learning generic representations with tremendous EEG data in BCI," *arXiv preprint arXiv:2405.18765*, 2024.